fire

MDPI

Article

A Fireline Displacement Model to Predict Fire Spread

Domingos X. Viegas *, Carlos Ribeiro, Thiago Fernandes Barbosa, Tiago Rodrigues and Luís M. Ribeiro

Department of Mechanical Engineering, University of Coimbra, ADAI, Rua Luís Reis Santos, Pólo II, 3030-788 Coimbra, Portugal; carlos.ribeiro@adai.pt (C.R.); thiago.barbosa@adai.pt (T.F.B.); tiago.rodrigues@adai.pt (T.R.); luis.mario@adai.pt (L.M.R.)
* Correspondence: xavier.viegas@dem.uc.pt

Abstract: Most current surface fire simulators rely upon Rothermel's model, which considers the local properties of fuel, topography, and meteorology to estimate the rate of spread, and utilises the concept of elliptical growth to predict the evolution of the fire perimeter throughout time. However, the effects of convective processes near the fireline, which modify fire spread conditions along the fire perimeter, are not considered in this model. An innovative fire prediction simulator based on the concept of fireline element displacement, which is composed of translation, rotation, and extension, rather than a point-by-point displacement, is proposed in this article. Based on the laws of convective heat fluxes across and along the fireline and on laboratory experiments, models to estimate the angular rotation velocity and the extension of the fireline during its displacement are proposed. These models are applied to a set of laboratory experiments of point ignition fires on slopes of 30° and 40° and, given the fact that the rate of spread of the head, back, and flank fire are known, the evolution of the fire perimeter can be predicted. The fire spread model can be applied to other situations of varying boundary conditions provided that the parameters required by the model are known.

Keywords: fire behaviour; slope; topography and wind effects; fireline rotation; fireline extension; convective effects; prediction simulator

Citation: Viegas, D.X.; Ribeiro, C.; Barbosa, T.F.; Rodrigues, T.; Ribeiro, L.M. A Fireline Displacement Model to Predict Fire Spread. *Fire* **2024**, *7*, 121. https://doi.org/10.3390/fire7040121

Academic Editors: Yanming Ding, Kazui Fukumoto and Jiaqing Zhang

Received: 7 February 2024
Revised: 21 March 2024
Accepted: 26 March 2024
Published: 6 April 2024

1. Introduction

The modelling of forest fire propagation has been the subject of extensive research using different methodologies to address this very complex phenomenon. In [1–5], a comprehensive analysis of fire behaviour modelling can be found. Given its prevalent nature, surface fire behaviour is the object of many studies aiming to produce fire prediction models to estimate the development of a fire under arbitrary conditions. A large number of these models and their fire prediction systems [6–12] use the semi-empirical approach based on the model proposed by Rothermel [13] and extended upon with the Behave System [14,15].

The Rothermel model is based on a large database of laboratory scale experiments, using a wide set of fuel beds under controlled slope or wind conditions. A mathematical model based on the statistical analysis of experimental data is proposed to estimate the basic rate of spread of a fire under no slope and no wind conditions. Assuming an additive vectorial effect of slope and wind, correction functions to adjust for the influence of either slope or wind are proposed. Given the limited nature of the experimental conditions, these equations can only be applied strictly to predict the head fire rate of spread (ROS) in the direction of the slope gradient or wind vectors.

The Rothermel model assumes that the ROS value is defined by the local properties of the fuel bed, the slope, and the wind. As local convective processes induced by the fire are not involved, the dynamic behaviour of the fire is not considered in the model. Therefore, if the local properties remain constant, the value of the ROS will also be constant. In [16] it was shown that even in nominally permanent and uniform boundary conditions, in general cases, the ROS value varies with time, as the case of the eruptive fire illustrates very well [17,18].

Despite these limitations and the absence of analysis regarding the evolution of the ROS in different directions, ref. [14] assumes that a point fire ignition on a slope or under permanent wind conditions spreads taking a form that is well described by a simple or a double ellipse. To the knowledge of the present authors, the concept of elliptical growth was never validated in the sense of justifying why a point ignition fire develops from an initial circular form to an ellipse or to any other of the many shapes that are found in fire perimeters. Several authors recognize that different shapes, including rectangles, can be used to approximate the perimeters of real fires [19,20].

Based on the Huygens principle, the fire perimeter spread was estimated by modelling it as the propagation of a wave, defined by a series of ellipses corresponding to the spread of point-ignited fires at each location at the fire perimeter [21–25]. Various mathematical models and fire behaviour prediction systems have refined the ellipse-shaped fire propagation model by incorporating additional variables [6,11,26,27]. Although the ellipse-shaped propagation approach remains useful, these models do not fit well with the linear shape of the straight fireline that are observed in many fires.

As shown in [28], a non-horizontal fireline spreading on a uniform slope does not spread parallel to itself, prompting the author to define a rotational movement of the fireline. Based on laboratory and field experiments, as well as on the analysis of real fires, it was shown that this lack of uniformity of the local rate of spread—contradicting the Rothermel model—is due to the transverse convection along the fireline, which modifies the ROS value along its length. This concept was extended for wind driven fires in [29] and used to show that the fire perimeter is not always a regular line, but instead can assume patterns which are referred to as zigzag shapes [30]. In [31], the spread of backfires at a laboratory scale in slope or wind conditions was analysed. A semi-empirical model to estimate the rotational velocity of the fireline was proposed in [32].

Given the necessity to account for convective processes at the fire front near each point, the present work adopts the concept of fireline displacement to predict the evolution of the fire front as opposed to a point-by-point approach. This involves reviewing previously proposed concepts of fireline rotation and extension as well as developing a new formulation for the extension laws. The fireline displacement model validated through testing with the predictions of point ignition fires from laboratory experiments conducted with uniform fuel beds on different slopes. The model explains the continuous evolution of a point ignition fire to the shapes that are observed in the experiments and will be used as a learning tool to create a library of parameters enhancing its applicability to a wider set of boundary conditions.

2. Fireline Displacement Model

Current fire spread simulators (which are used to predict fire behaviour) rely on knowing the components of the rate of spread (ROS) vector at each point of the fireline over time. The most common modelling approach for estimating local ROS is the one proposed by Rothermel [13], which assumes that the ROS at any given point depends solely on local properties such as slope, fuel cover, and wind velocity. Among other limitations, this model overlooks the convective processes generated by the fire as a whole as well as those from neighbouring sections of the fireline. Recognizing the challenges associated with determining the ROS at each point along the fire perimeter, an alternative approach is proposed which involves leveraging empirical data or models to determine the ROS values at the head, flank, and back of the fire.

2.1. Modeling Approach

The present modelling approach addresses the common scenario of a fire originating at a single point that spreads in the landscape forming a closed line perimeter, with a well-defined head fire, two flanks, and a tail (Figure 1). In this general scenario, the line representing the head fire will typically be a curved line and its ROS value will be a function of time $\vec{R}_1(\mathrm{t})$. The same will happen with the rear fire $\vec{R}_2(\mathrm{t})$ and the flanks ($\vec{R}_{3l}(\mathrm{t})$ and $\vec{R}_{3r}(\mathrm{t})$). Assuming that the values of these functions are known, the evolution of four designated reference points of the fire front—$\mathbf{Q_1}$, $\mathbf{Q_2}$, $\mathbf{Q_3}$, and $\mathbf{Q_4}$—can be estimated over time, as is shown in the figure for two steps of time. The prediction of the evolution of the fire perimeter requires the knowledge of the position of each element of the fireline. The present modelling approach assumes that the positions of the four reference points $\mathbf{Q_i}$ are known at each time step and can be used as anchor points to determine the evolution of the remaining elements of the fireline.

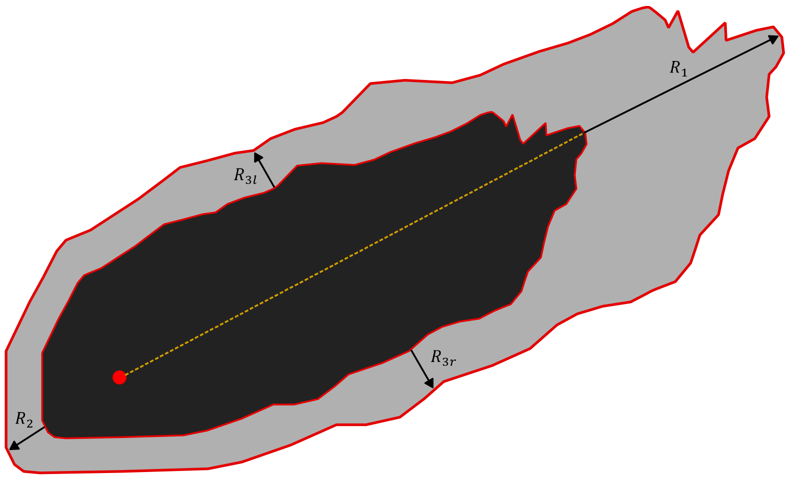

Figure 1. General view of fire with a single point ignition spreading along main direction. The dashed line represents the main axis of head fire front propagation.

To simplify our approach, we consider the case shown in Figure 2, where a fire is ignited on a homogeneous fuel bed on a flat surface, with either constant wind flow or uniform slope. In this scenario, the path of the head fire forms a straight line, which is a symmetry line for the fire perimeter.

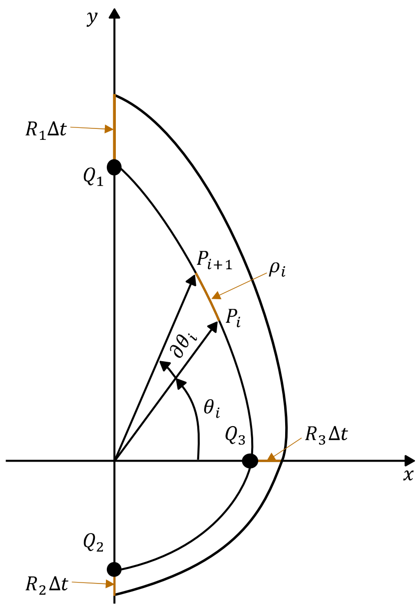

Figure 2. Schematic view of fire perimeter of a point ignition fire spreading under constant and uniform wind or slope conditions. Reference points $\mathbf{Q_1}$, $\mathbf{Q_2}$, and $\mathbf{Q_3}$ are shown.

To model the evolution of the fire front, the fire perimeter was divided into a number of n fireline elements (FLEs), and the movement of each was predicted in a succession of time steps Δt.

Reference FLE—four references FLEs centred on the points $\mathbf{Q_1}$, $\mathbf{Q_2}$, $\mathbf{Q_3}$, and $\mathbf{Q_4}$ were selected. The evolution of these reference elements is known, and they can be used as anchors to define the position of the other elements of the fireline. To ensure that the partition of the fireline includes these reference FLEs, it was proposed that the number of fireline elements is a multiple of four: $n = 4k$, k being an integer number.

Each fireline element $\boldsymbol{E_i}$ is defined by its start and end points, denoted as $\mathbf{P_i}(x_i, y_i)$ and $\mathbf{P_{i+1}}(x_{i+1}, y_{i+1})$ respectively. The length and inclination of each element in relation to the driving force that is moving the fire (wind or slope) are determined by:

$$s_i = \sqrt{(y_{i+1} - y_i)^2 + (x_{i+1} - x_i)^2}, \tag{1}$$

$$\beta_i = atan\left(\frac{y_{i+1} - y_i}{x_{i+1} - x_i}\right). \tag{2}$$

A radial coordinate was introduced for each point, defined as:

$$\theta_i = atan\left(\frac{y_i}{x_i}\right). \tag{3}$$

To simplify the modelling, the fire perimeter was divided into sections based on the quadrants in Figure 2. Due to the symmetry of the problem, only Section 1 in quadrant 1: ($0° < \theta < 90°$) and Section 2 in quadrant 4: ($-90° < \theta < 0°$) were considered, with the assumption that the other two are identical.

2.2. Displacement of a Fireline Element

Let us consider a fireline element limited by points $\mathbf{P}_1$ and $\mathbf{P}_2$ at a given time and analyse its displacement during the time interval Δt (Figure 3). A local coordinate system was defined where the OX axis coincides with element $\mathbf{P}_1$ and $\mathbf{P}_2$. The coordinates of these points are $\mathbf{P}_1(0, 0)$ and $\mathbf{P}_2(\mathrm{s}, 0)$.

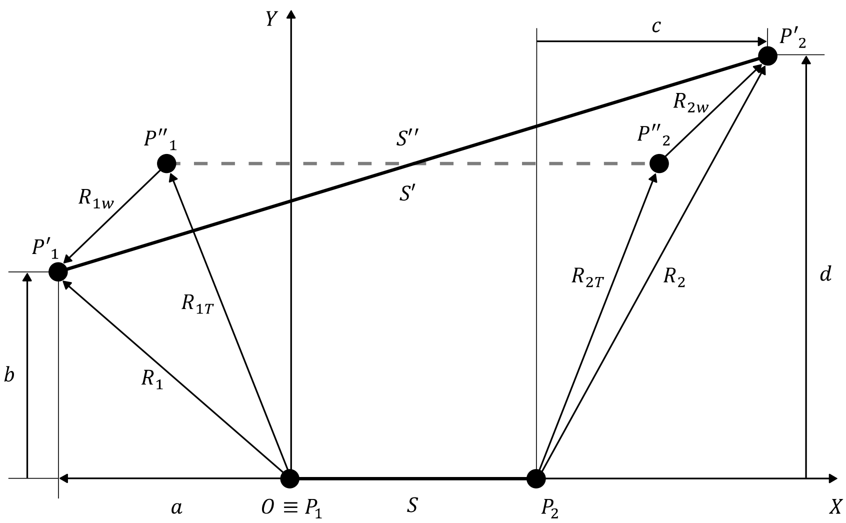

Figure 3. Illustrates displacement of a FLE represented by points $\mathbf{P_1}$ and $\mathbf{P_2}$ under arbitrary spreading conditions, consisting of a translation followed by a rotation.

The local ROS vectors at these points are:

$$\vec{R_1} = a.\vec{e_1} + b.\vec{e_2}, \tag{4}$$

$$\vec{R_2} = c.\vec{e_1} + d.\vec{e_2}. \tag{5}$$

The following auxiliary pair of vectors, designated as translation and rotation vectors, respectively, are defined as:

$$\vec{R_{1T}} = \frac{a-c}{2}.\vec{e_1} + \frac{b+d}{2}.\vec{e_2}, \tag{6}$$

$$\vec{R_{2T}} = \frac{c-a}{2}.\vec{e_1} + \frac{b+d}{2}.\vec{e_2}, \tag{7}$$

$$\vec{R_{1\omega}} = \frac{a+c}{2}.\vec{e_1} + \frac{b-d}{2}.\vec{e_2}, \tag{8}$$

$$\vec{R_{2\omega}} = \frac{a+c}{2}.\vec{e_1} + \frac{d-b}{2}.\vec{e_2}. \tag{9}$$

It can be seen that $\vec{R_{1T}} + \vec{R_{1\omega}} = \vec{R_1}$ and $\vec{R_{2T}} + \vec{R_{2\omega}} = \vec{R_2}$. It should be noted that the components of these ROS vectors represent linear velocities (m/s) (or cm/s in the present analysis). To convert them into linear distances, it is necessary to multiply them by the time interval Δt(s) of the analysis.

The displacement of element $\overline{\mathbf{P_1 P_2}}$ can be decomposed in a translation to $\overline{\mathbf{P''}_1\mathbf{P''}_2}$ followed by a rotation, to become $\overline{\mathbf{P'}_1\mathbf{P'}_2}$, as indicated in Figure 3.

Designating the position vector of point $\vec{\mathbf{P}_i}$ by $\mathbf{P_i}$, it can be written as:

$$\begin{bmatrix} \vec{\mathbf{P'}_1} = a.\Delta t.\vec{e_1} + b.\Delta t.\vec{e_2} \\ \vec{\mathbf{P'}_2} = (s + c.\Delta t).\vec{e_1} + d.\Delta t.\vec{e_2} \end{bmatrix} \tag{10}$$

$$\begin{bmatrix} \vec{\mathbf{P''}_1} = \left(\frac{a-c}{2}\right).\Delta t.\vec{e_1} + \left(\frac{b+d}{2}\right).\Delta t.\vec{e_2} \\ \vec{\mathbf{P''}_2} = \left[s + \left(\frac{c-a}{2}\right).\Delta t\right].\vec{e_1} + \left(\frac{b+d}{2}\right).\Delta t.\vec{e_2} \end{bmatrix}. \tag{11}$$

2.3. Analysis of Fireline Extension

It can be shown that the total extension of the FLE is given by:

$$ds = s' - s = \left(s' - s''\right) + \left(s'' - s\right) = ds_T + ds_\omega. \tag{12}$$

The FLE extension coefficient is defined by:

$$\varepsilon = \frac{ds}{s.\Delta t}. \tag{13}$$

From Equations (1), (12), and (13), the values of s', ds, and ε can be determined:

$$s' = \sqrt{[s + (c-a).\Delta t]^2 + [(d-b).\Delta t]^2}, \tag{14}$$

$$ds = \sqrt{[s + (c-a).\Delta t]^2 + [(d-b).\Delta t]^2} - s, \tag{15}$$

$$\varepsilon = \frac{ds}{s.\Delta t} = \sqrt{\left[\frac{1}{\Delta t} + \frac{(c-a)}{s}\right]^2 + \left[\frac{d-b}{s}\right]^2} - \frac{1}{\Delta t}. \tag{16}$$

Let us define X associated to translation and Y associated to rotation:

$$X = \left|\frac{c-a}{s}\right|, \tag{17}$$

$$Y = \left|\frac{d-b}{s}\right|. \tag{18}$$

For a given value of Δt, ε can be defined as a function of both X and Y:

$$\varepsilon = \frac{ds}{s.\Delta t} = \sqrt{\left[\frac{1}{\Delta t} + X\right]^2 + Y^2} - \frac{1}{\Delta t}. \quad (19)$$

As parameters X and Y are associated with the translation and the rotation of the FLE, respectively, it can be concluded that, in the general case, the extension coefficient has both a rotation and a translation component. This relationship is shown in Figure 4 where the values of ε are plotted for fixed values of Δt equal to 15 s and 20 s, as a function of X for given values of Y. As can be seen, if $Y = 0$, ε is equal to X. In the other cases, it varies with both X and Y.

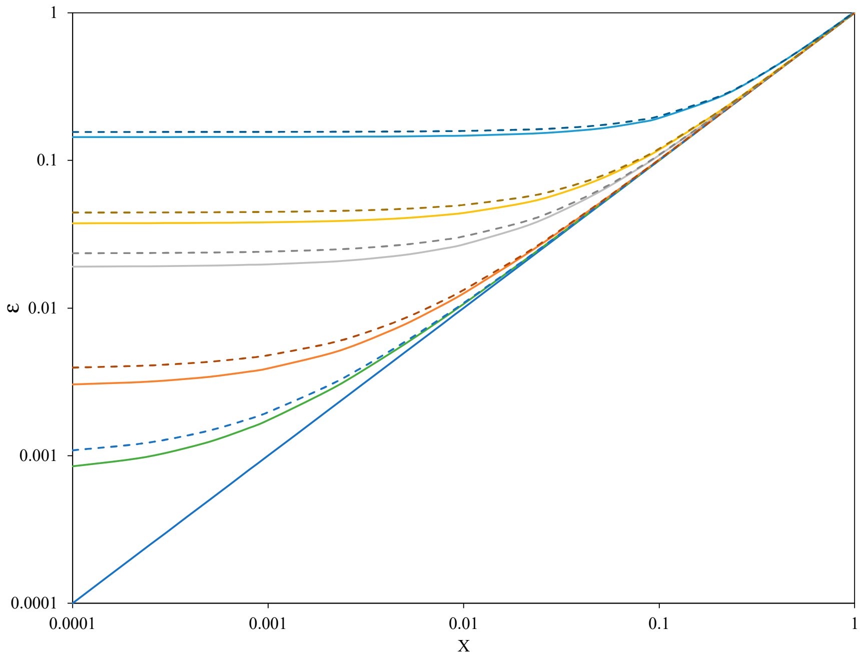

Figure 4. Variation of extension coefficient ε as a function of X for predefined values of Y and two values of Δt: continuous line Δt = 15 s and dotted line Δt = 20 s.

Note that in [32] the analysis of the fireline displacement was incorrect. It was erroneously assumed that the components a − c = c − a = 0, which represents a specific case depicted in Figure 3.

2.4. Estimation of Local Value of Fireline Extension

To estimate the value of ε for each FLE, the local ROS at each point of the FLE must be known. Three adjacent FLEs—E_{i-1}, E_i, and E_{i+1}—make the angles β_{i-1}, $\beta_{i,}$ and β_{i+1}, respectively, with the OX axis (see Section 2.4.2). The modulus and direction of the local values of the ROS were estimated at points $\mathbf{P_i}$ and $\mathbf{P_{i+1}}$.

2.4.1. Approximate Value of the Modulus of the ROS

According to the present approach, the local values of the ROS are known only for:

$$\text{Head fire } \theta = 90^\circ \rightarrow R = R_1, \quad (20)$$

$$\text{Lateral fire } \theta = 0^\circ \rightarrow R = R_3, \quad (21)$$

$$\text{Backfire } \theta = -90^\circ \rightarrow R = R_2. \quad (22)$$

It is assumed that the ROS modulus varies continuously along the perimeter of the fireline. For each point $\mathbf{P_i}(x_i, y_i)$ of the fireline perimeter, the angular coordinate ξ was defined based on the position angle θ, as defined by Equation (4):

$$\xi = \frac{2.\theta}{\pi} \tag{23}$$

Among the various possible functions that can be used to represent the variation of the modulus of the ROS along the fire perimeter, the following set of equations to describe the variation of the modulus R of the ROS with θ or ξ was proposed:

$$0 < \theta < \frac{\pi}{2} \rightarrow R = R_3 + (R_1 - R_3).\xi^{m_1}, \tag{24}$$

$$-\frac{\pi}{2} < \theta < 0 \rightarrow R = R_3 + (R_2 - R_3).(-\xi)^{m_2}, \tag{25}$$

m_1 and m_2 were considered as empirical parameters of the model that have to be defined for the first and the fourth quadrants, respectively.

Assuming values of R_1 = 1.2 cm/s, R_2 = 0.4 cm/s, and R_3 = 0.6 cm/s, Figure 5 shows the evolution of R according to Equations (24) and (25) for the indicated values of m_1 or m_2. As shown in this figure, the one-parameter power function used in this model can produce a wide range of variations of the ROS along the perimeter. For low values of m, starting from θ = 0°, the modulus of R remains close to R_3 for increasing or decreasing values of θ, and then changes rapidly to either R_1 or R_2 while the opposite happens for large values of m.

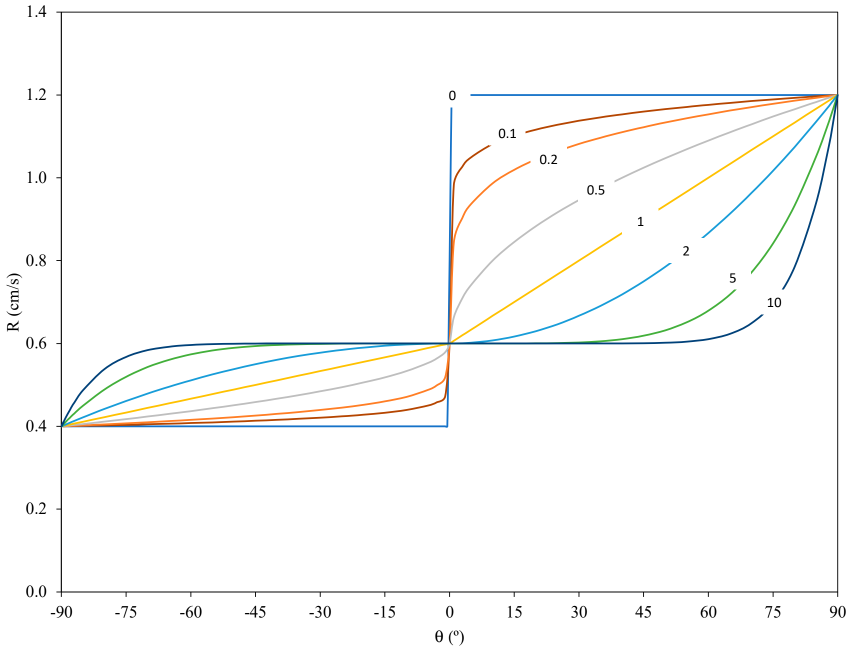

Figure 5. Variation of modulus of ROS along fireline perimeter, according to Equations (24) and (25), for given values of parameters m_1 and m_2. Values of R_1, R_2 and R_3 are only indicative.

2.4.2. Approximate Value of the Direction of the ROS

It was assumed that the direction of the ROS vector R_i at point $\mathbf{P_i}$ coincides with the bisector of the lines perpendicular to the two adjacent FLEs E_{i-1} and E_i (Figure 6). It is possible to show that the angle between these two lines is given by $\beta_i - \beta_{i-1}$, therefore the components of R_i and R_{i+1} can be determined:

$$\begin{array}{l} a_i = -|R_i|.\sin\left(\frac{\beta_i - \beta_{i-1}}{2}\right) \\ b_i = |R_i|.\cos\left(\frac{\beta_i - \beta_{i-1}}{2}\right) \end{array}, \tag{26}$$

$$\begin{aligned} c_i &= |R_{i+1}|.\sin\left(\frac{\beta_{i+1}-\beta_i}{2}\right) \\ d_i &= |R_{i+1}|.\cos\left(\frac{\beta_{i+1}-\beta_i}{2}\right) \end{aligned}. \tag{27}$$

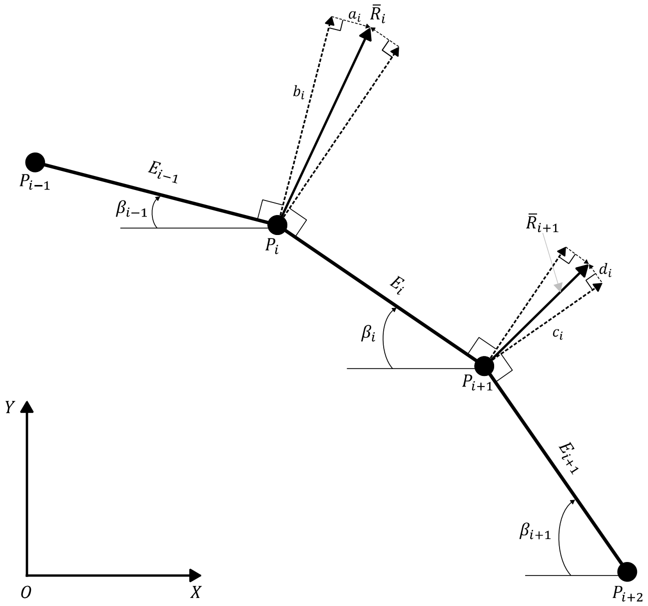

Figure 6. Schematic representation of three consecutive FLEs with respective inclination angles $\beta_{\rm i}$ and ROS vectors at points $\mathbf{P_i}$ and $\mathbf{P_{i+1}}$.

To estimate the FLE extension coefficient for each FLE, components a_i, b_i, c_i, and d_i were calculated using Equations (26) and (27). The values of X and Y were then computed using Equations (17) and (18). Finally, knowing the value of Δt, the ε coefficient was calculated using Equation (19). To account for the approximate nature of the present approach, a correction coefficient k_E to evaluate the values of ε_c in any given step of the calculation is used:

$$\varepsilon_c = k_E.\varepsilon. \tag{28}$$

2.4.3. Extension of the Reference Element Containing $\mathbf{Q_1}$

It was found that when using the present model to estimate the extension of the element E_1 that contains the reference point $\mathbf{Q_1}$, assuming that this element remains parallel to itself (β = 0°), the rotation of the second element E_2 creates a very large difference in the values of a and c, resulting in a high value of the ε coefficient for this FLE. To overcome this problem, it was assumed that the extension coefficient of this element follows a law similar to that of an element of the fireline with uniform ROS that was analysed in [32], yielding:

$$\varepsilon_o = \frac{k_o}{t}. \tag{29}$$

In this equation, k_o is a constant that can be estimated at the beginning of fire spread or adjusted to achieve a better overall agreement between the model and the experimental results.

2.5. Fireline Rotation Law

The problem of fireline element rotation was analysed in [32]. Considering the convective flow induced by the presence of a non-horizontal fireline on a slope, it was shown that there is a variation of the ROS along the fireline that produces the rotation of the fire front.

Assuming that the ROS variation due to the flow component u_y perpendicular to the FLE is given by the following empirical law:

$$R = R_o.\left(1 + a_1.u_y{}^{b_1}\right), \quad (30)$$

and that the increase of the u_y component along the OX axis due to the cross flow u_x induced along the fireline element is given by:

$$\frac{du_y}{dx} = a_3.u_x{}^{b_3}. \quad (31)$$

The following law for determining the rotational velocity of a given FLE was deduced:

$$\omega = \frac{d\beta}{dt} = R_o.a_1.b_1.a_3.u_y{}^{b_1-1+b_3}.(cos\beta)^{b_1-1}.(sin\beta)^{b_3}. \quad (32)$$

The units of ω are °/s. The parameters a_1 and b_1 in Equations (30) and (32) depend on the fuel bed properties and can be determined from independent experimental tests. In the case of fuel beds composed of dead needles of *Pinus pinaster* needles, the following values were determined: a_1 = 3.54; b_1 = 2.14 [32]. The units of a_1 are complex but the numerical value indicated corresponds to the u_y expressed in m/s.

The values of a_3 and b_3 in Equation (31) depend on the fire spread conditions. In [32], it is reported that for tests with pine needles on a slope, the following values were obtained: for a 30° slope: a_3 = 58.1° and b_3 = 0.29; for a 40° slope: a_3 = 128.2° and b_3 = 0.45.

The Equation (32) can be written in the following form:

$$\omega = A_w.(|cos\beta|)^{b_1-1}.(|sin\beta|)^{b_3}. \quad (33)$$

To avoid problems in the evaluation of ω using Equation (33), the modulus of the trigonometric functions is utilised. In this equation, A_w (°/s) is an empirical parameter that encompasses the dependence on the local ROS—contained in R_o and u_y—as well as the other empirical coefficients a_1, b_1, and a_3, which will be determined for the present set of experiments and its value adjusted in the simulation model.

Using the values of the model parameters, the shape of the function given by Equation (33) for fire spread in pine needles in 30° and 40° slopes is shown in Figure 7, with A_w = 1 °/s.

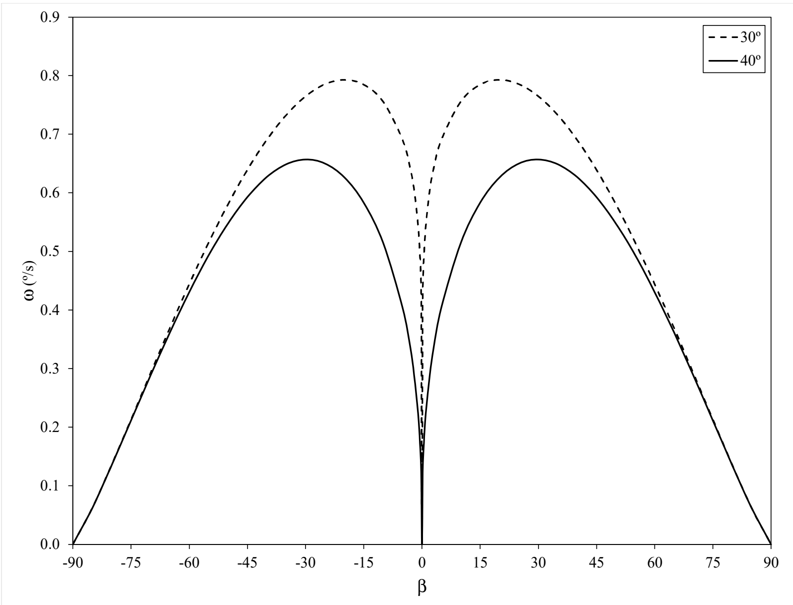

Figure 7. Evolution of fireline rotation velocity according to present model for slopes of 30° and 40° using A_w = 1°/s.

3. Materials and Methods

3.1. Laboratory Experiments

The laboratory experiments were conducted at the Forest Fire Research Laboratory (LEIF) at the University of Coimbra in Lousã. The tests with a point ignition fire on a slope were conducted on the Canyon Table DE4, as described in [32]. The table measures 6×8 m^2 and can be inclined from 0 to 40 degrees. In the tests, a rectangular fuel bed measuring 2×6 m^2 composed of dead needles of *Pinus pinaster* with a load of 0.6 kg/m^2 (dry basis) was used. These tests followed protocols and methodologies described in previous works by the team [16,33,34].

Continuous images from each experiment were captured by an infra-red camera, specifically the FLIR T1020. Although the optical axis of the camera was almost perpendicular to the fuel bed, an algorithm was applied to correct the images in a selected set of frames from each test. The experimental program consisted of several tests with varying slope angles, all yielding very similar results. As the purpose of the present work is to validate a fire perimeter evolution prediction model, one test with a slope of 30° and another with a slope of 40° were considered. Frames from the tests with a slope of 30° and 40° are shown in Figures 8 and 9, respectively.

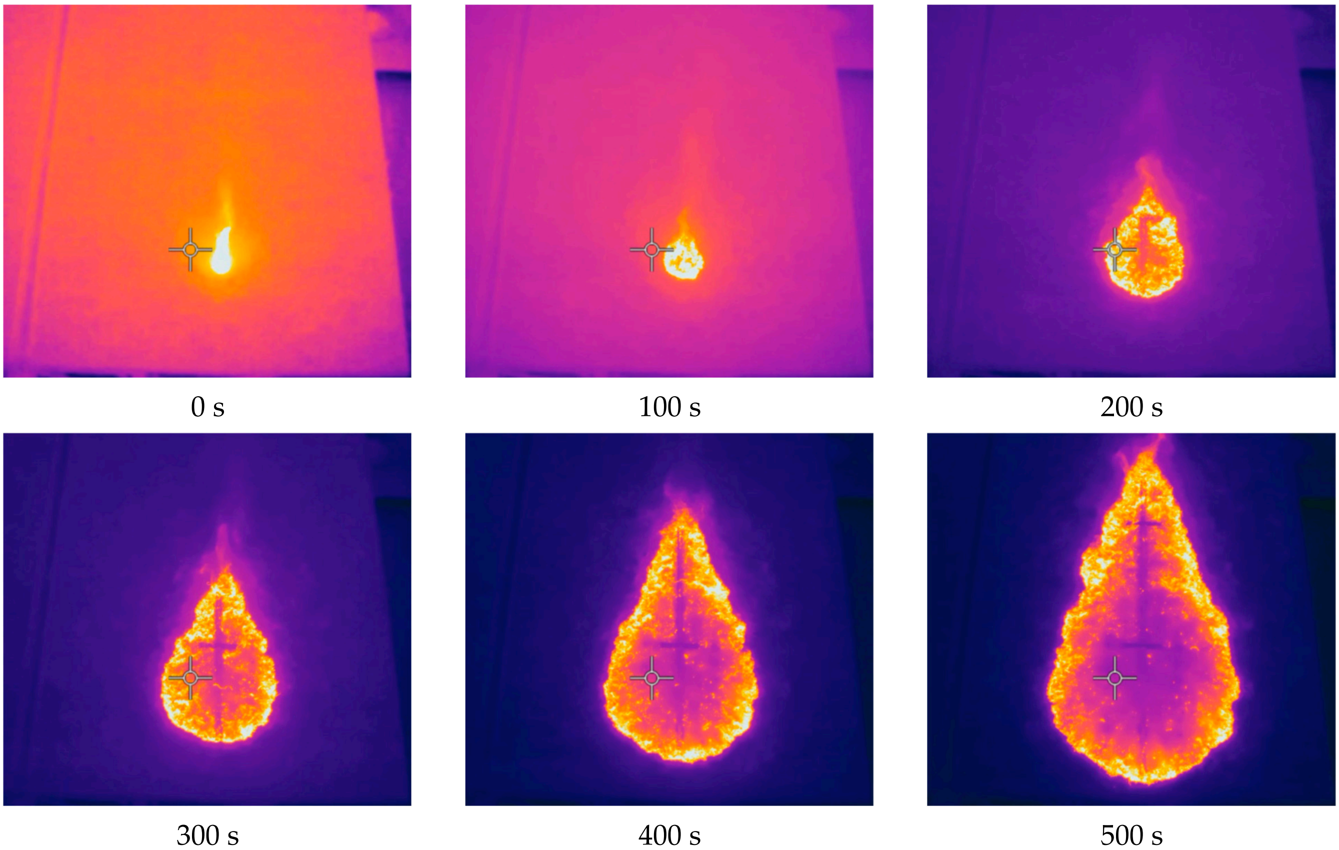

Figure 8. Infrared images of fire spread for a point ignition fire with 30° slope.

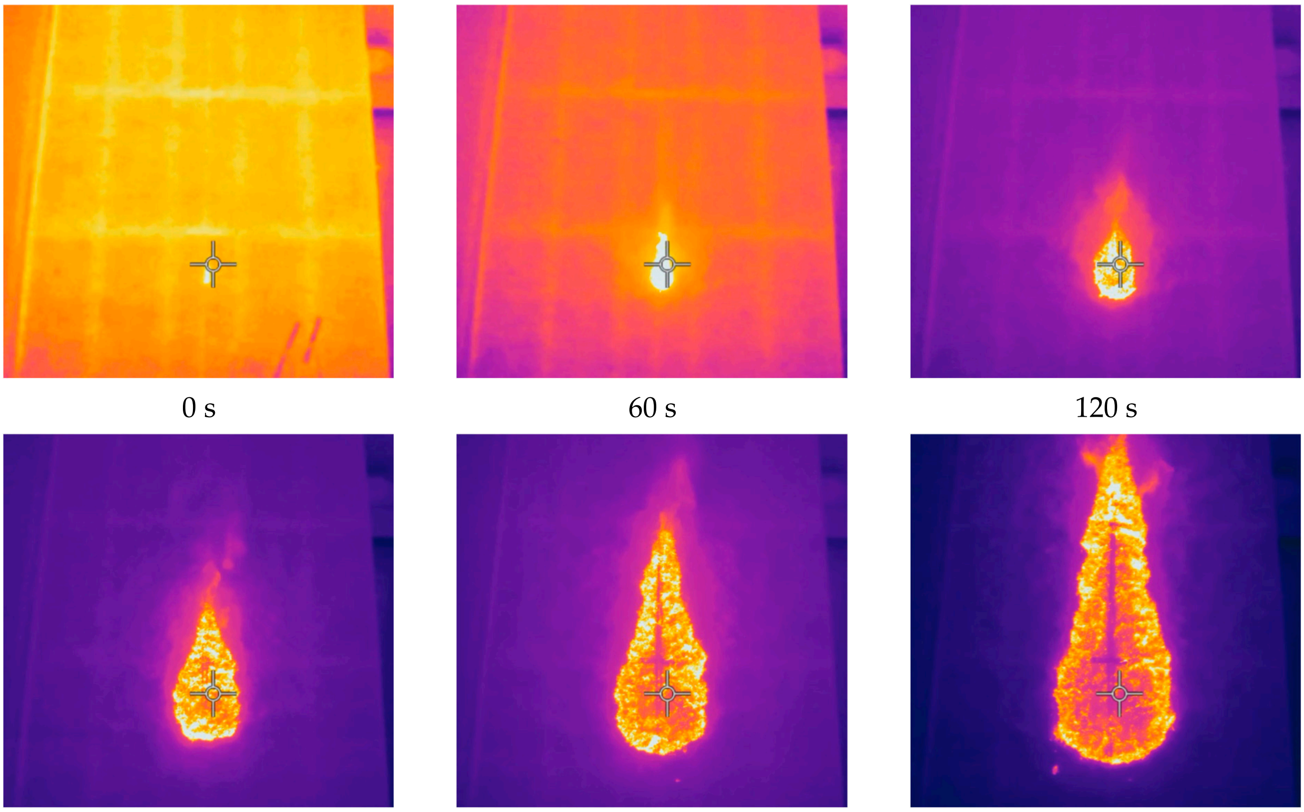

Figure 9. Infrared images of fire spread for a point ignition fire with 40° slope.

3.2. Numerical Model

To implement the model, it was assumed that at a given starting time, denoted as t_0, the fire perimeter is represented by a circle of radius R_o. The circle was divided into $n = 4k$ elements so that the four reference elements, centred at points $\mathbf{Q_1}$ to $\mathbf{Q_4}$ as defined above, are included in the simulation, as their ROS is assumed to be known.

To facilitate the geometrical representation and the description of the calculation process, 32 elements of the fire perimeter ($k = 8$) were initially considered, but the implementation method can be used with any other numbers of elements. This initial perimeter is shown in Figure 10. The reference elements in this case are E_1, E_9, E_{17}, and E_{25}. They are divided into two elements each. For example, E_1, is divided into E_{1A} ($\mathbf{Q_1}$, $\mathbf{P_1}$) and E_{1B} ($\mathbf{P_{36}}$, $\mathbf{Q_1}$), and so they must be treated separately as they are under different fire spread conditions, as described below.

The calculation process will be presented. This process aims to estimate the coordinates of each FLE after its displacement in a given time step. The calculation is based on the proposed partition of the fireline into 32 FLEs.

To evaluate the individual displacement of each FLE in each time step Δt, the upslope (head fire) and the downslope (backfire) propagation Sections 1 and 2, in sectors 1 and 2, were calculated separately as they are governed by different physical conditions. Each section will be divided into two subsections that are calculated sequentially to define the adjustment criteria of the model parameters. As the fireline in Section 1 propagates in the same direction as the head fire, the letter "H" will be assigned to the parameters associated with this section of the fireline. Conversely, the letter "B" will be assigned to the parameters associated with the backfire.

The simulation progresses step-by-step from the initial time ($t = 0$ s) until the final time (t_{fin}). The fixed value of k_o was sued in Equation (29) for the entire calculation, and a constant value of time step Δt was assumed.

It is important to note that the present model relies on a set of empirical parameters K_o, A_w, k_e, and m_1, whose values are not precisely known in each case. Consequently, they have to be adjusted in order to obtain the best agreement between observations and model predictions.

Initially, the values of A_{wH}, k_{eH}, and m_1 for each time step were fixed and then adjusted, as explained below.

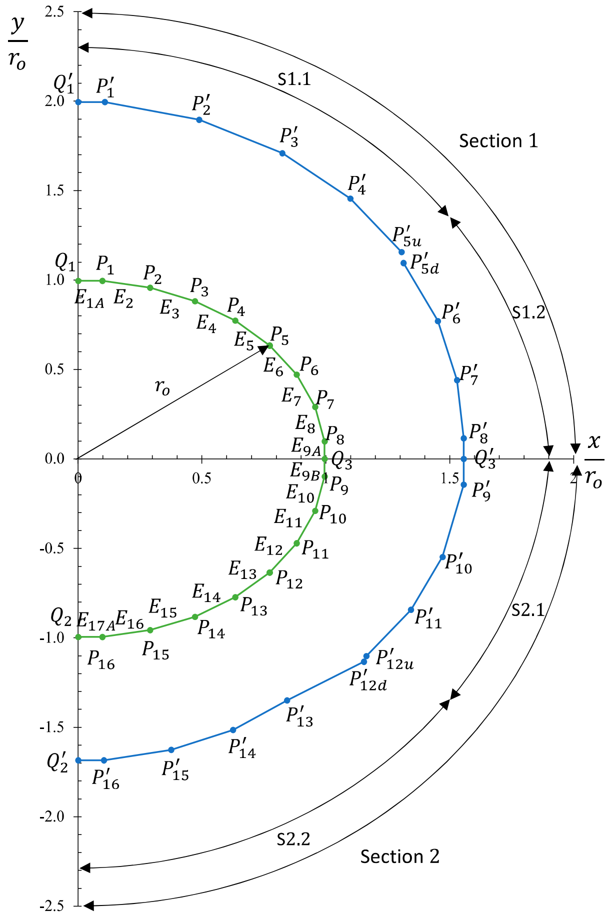

Figure 10. Schematic presentation of perimeter of fire, divided into 32 FLEs at time of ignition and at time $t + \Delta t$. Each section (1 and 2) is divided into two subsections (S1.1, S1.2 and S2.1, S2.2).

3.2.1. Calculation of Section 1

Section 1 of the fire perimeter is divided into two subsections: S1.1, consisting of FLEs E_1, E_2, E_3, E_4, and E_5; and subsection S1.2, consisting of E_6, E_7, E_8, and E_{9a}, which represents the upper part of element E_9.

Subsection S1.1

Subsection S1.1 commences with element E_{1a}, wherein its displacement and extension are calculated. It is assumed that this element does not rotate. Its point $\mathbf{Q_1}(0, y_{Q1})$ moves along the OY axis at the distance given by $R_1.\Delta t$.

As defined above, the extension coefficient of this fireline element is k_o/t, with a predefined value of k_o. Therefore, the extension of this fireline element will be:

$$ds_{1a} = s_{1a}.\frac{k_o}{t}.\Delta t. \tag{34}$$

Therefore, its length at time $t' = t + \Delta t$ will be:

$$s'_{1a} = s_{1a} + ds_{1a}. \tag{35}$$

The extremities of E'_{1a} are points $\mathbf{Q'_1}$ $(0, y_{Q1} + R_1.\Delta t)$ and $\mathbf{P'_1}(s'_{1a}, y_{Q1} + R_1.\Delta t)$.

Proceeding to element E_2, its rotation dβ_2 was determined using Equation (33) and β'_2 was calculated as:

$$\beta'_2 = \beta_2 + \omega(\beta_2).\Delta t. \tag{36}$$

To estimate the extension of E_2, the components of a_2, b_2, c_2, and d_2, according to Equations (26) and (27), need to be calculated along with the known position of this element in the previous time step. By calculating the respective extension coefficient ε_2, the s'_2 length of the FLE at time $t + \Delta t$ can be estimated. Subsequently, the coordinates of the other extremity of E'_2, point $\mathbf{P'_2}(x'_2, y'_2)$ that are given, can be obtained:

$$x'_2 = s'_{1a} + s'_2.cos\beta'_2, \tag{37}$$

$$y'_2 = y'_{1a} - s'_2.sin\beta'_2. \tag{38}$$

Similar calculations are performed for FLEs E_3, E_4, and E_5. FLE E'_5 is limited by points $\mathbf{P'_4}$ and $\mathbf{P'_{5d}}$, which are important to adjust the model parameters. This point is designated as $\mathbf{P'_{5d}}$ because it derives from a calculation that starts from the top of the fireline and progresses downward, with decreasing values of θ.

Subsection S1.2

To conclude Section 1 of the fireline, the displacement of its subsection S1.2, composed of FLEs, E_6, E_7, E_8, and E_{9a} is calculated. It commences with FLE E_{9a} and progresses upwards with increasing θ until FLE E_6.

FLE E_{9a} displaces parallel to itself with a ROS R_3, making the coordinates of point $\mathbf{Q'_2}$ $(x_{Q2o} + R_3.\Delta t, 0)$. The extension coefficient ε_{9a} is determined according to the model using Equations (19) and (28), and the coordinates of point $\mathbf{P'_8}$ are given by $(x_{Q2o} + R_3.\Delta t, s'_{9a})$. For element E_8, as with all others except for E_{1a}, the extension coefficient is calculated according to the proposed model to determine the coordinates of $\mathbf{P'_7}$ and subsequent points up to point $\mathbf{P'_{5u}}$, calculated proceeding upwards from the OX axis.

It is worth noting that points $\mathbf{P'_{5u}}$ and $\mathbf{P'_{5d}}$ will coincide in this initial calculation step. By adjusting the values of A_w, K_e, and m_1, these points can be aligned to the required precision. In this study, an Excel sheet was used to make the calculations and a plot of the fireline was inspected visually to check the alignment of the two points. Typically, this was achieved by adjusting the first two parameters, and it was observed that the model was not sensitive to small variations of m_1.

An automatic method to determine the location of the points $\mathbf{P}_{5u}$ and $\mathbf{P}_{5d}$ or $\mathbf{P}_{12u}$ and $\mathbf{P}_{12d}$ was implemented. We imposed the condition that the distance between $\mathbf{P}_{5u}$ and $\mathbf{P}_{5d}$ or $\mathbf{P}_{12u}$ and $\mathbf{P}_{12d}$ is less than 0.5 cm, and with this the parameters were automatically estimated, fulfilling this condition. The final values of the model parameters for this time step are those used in the adjustment process.

3.2.2. Calculation of Section 2

Similar to Section 1, Section 2 was divided into two subsections, and the displacement of the respective fireline elements were calculated sequentially. For subsection S2.1, composed of FLEs E_{17a}, E_{16}, E_{15}, and E_{14}, the calculation proceeds from bottom to top, while for subsection S2.2, composed of FLEs E_{13}, E_{12}, E_{11}, E_{10}, and E_{9b}, the calculation proceeds from top to bottom.

Initial values of the model parameters A_{wB}, k_{EB}, and m_2 are set for each time step and adjusted in the same manner as Section 1.

In this section, the control points $\mathbf{P'_{12d}}$ and $\mathbf{P'_{12u}}$ are used to verify the accuracy of the model's closure. The final values of the model parameters are determined based on achieving satisfactory adjustment.

When both sections are calculated for the first step, the process continues to the next time step and repeats until reaching the t_{fin}, marking the end of the calculation process.

4. Results

4.1. Experimental Results

4.1.1. Rate of Spread Results

Based on the IR images of the tests such as those shown in Figures 8 and 9, the ROS values for the head fire R_1, the backfire R_2, and the flanks R_3 were estimated for each experiment. For the 30° slope experiment, a time step of 20 s was used between successive frames. For the 40° slope tests, a time step of 15 s was used. The corresponding results are shown in Figure 11a,b, respectively, for α = 30° and α = 40°. Assuming the existence of symmetry, the flank ROS values R_{3l} and R_{3r} were averaged as R_3.

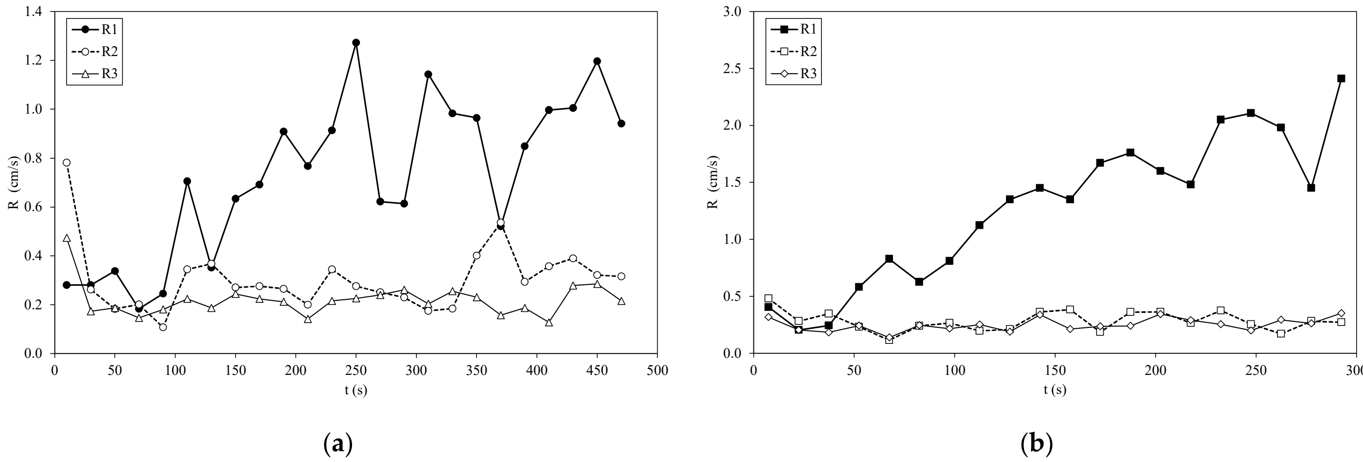

Figure 11. Experimental results of instantaneous values of ROS of head fire, R_1; backfire R_2; and flank fire, R_3. (**a**) Results for slope of 30°; (**b**) results for slope of 40°.

As can be seen in these figures, the ROS is not constant during the tests. According to the concept of oscillatory fire spread proposed in [34], variations in the ROS can be observed throughout the entire duration of the tests. In both cases, the amplitude of oscillations of the ROS of the back and the flank fires is not large, but that is not the case for the head fire R_1. For α = 30°, the value of R_1 increases in an oscillating process reaching around 1.5 cm/s (R' = 3.54) after 350 s, then decreases to 0.52 cm/s (R' = 1.24) and initiates a second acceleration cycle. For α = 40°, the value of R_1 increases steadily with oscillations, reaching a maximum value of 2.34 cm/s (R' = 5.80) after 290 s. It is possible that a deceleration would follow if the length of the table was larger in order to capture a second cycle of the fire oscillation. The results obtained with repetitions of these tests yield similar behaviour as what was already observed in [16].

These experiments demonstrate that it is incorrect to assume that the ROS values are constant during the propagation of single point ignitions, even with permanent and uniform boundary conditions, as assumed in [13]. In the absence of an accurate model to capture these oscillations and the fire growth, this work will utilise the results obtained in the experiments to model the evolution of the fire perimeter using the concepts of fireline rotation and extension.

4.1.2. Fireline Rotation Results

The movement of FLE along predefined directions was analysed in the tests conducted on slopes of 30° and 40° for both the upslope and the downslope sections of the fire. Consistent with the oscillatory character of the fire spread [16], oscillations were observed in the evolution of the inclination angle β of the FLE over time, resulting in a large scatter in the data, consistent with observations from previous studies [28,32,34].

The results obtained are shown in Figure 12a,b, for 30° and 40° slope, representing the upslope and downslope sections of the fireline, respectively.

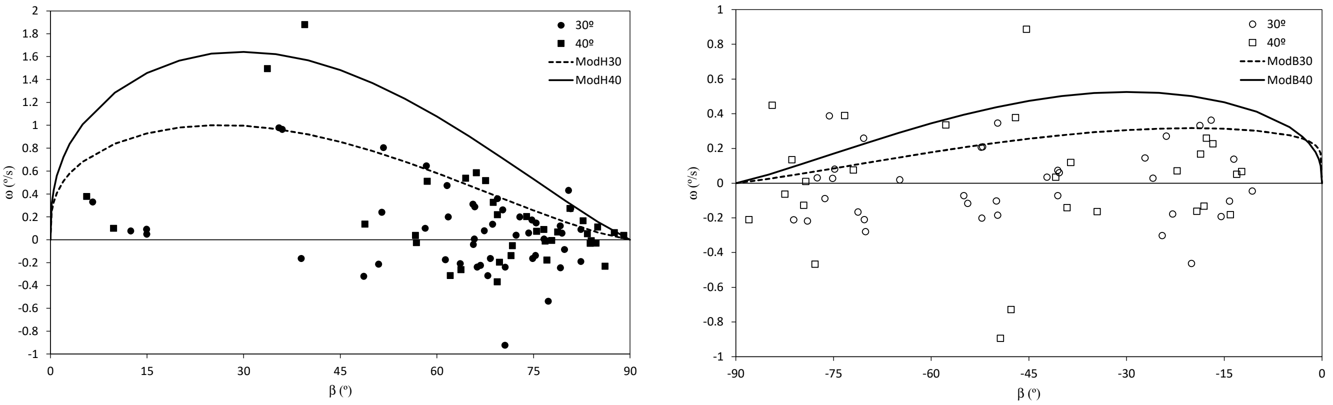

(**a**) (**b**)

Figure 12. Comparison between experimental results of fireline rotation law for slope angles of 30° and 40°. (**a**) Upslope or head fire section of the fireline, (**b**) downslope or backfire section of the fireline.

The values of A_w used to calculate the curves of the model in Figure 12 were equal to 1.5 and 2.5 for the 30° and 40° cases in the upslope fire, respectively, and equal to 0.4 and 0.8 for the cases in the downslope fire.

As can be seen in this figure, negative values for ω were measured in various cases, especially for the downslope section of the fire. At present, there is no explanation for this, as it corresponds to a negative effect of the induced local convection. More detailed studies are required to analyse the physical meaning of this result and to verify if it corresponds to the overall fluctuations of the fire spread that have been described in [33] (and that were also observed here).

As shown below, in the application of the model, negative values of A_w were used to adjust the shape of the fireline in some time steps.

4.2. Numerical Results

Using the numerical model described above, we were able to predict the evolution of the point ignition fire, employing the results of the tests to provide the values of R_1, R_2, and R_3 at each time step. This enabled us to replicate the observed transformation of the fire perimeter from the initial circular shape to the elongated form observed in the experiments.

Computation commenced at a time t_o = 0 in each case when the fire had formed a circle of R_o = 12.98 cm for α =30° and of R_o =6.04 cm for α = 40°. The time step used in the calculations matched the intervals mentioned above. The values of k_o were set as 0.60 for α = 30° and as 0.45 for α = 40°. The values of the model parameters A_w, k_E, m_1, and m_2 were adjusted during the calculation to follow the evolving of the instantaneous value of R_1 to ensure a precise representation of the figure, represented by the adjustment of points $\mathbf{P'_{5u}}$ and $\mathbf{P'_{5d}}$ or $\mathbf{P'_{12u}}$ and $\mathbf{P'_{12d}}$ as described above.

The results of the model predictions are shown in Figures 13 and 14 for α = 30° and α = 40°, respectively. The isochrones with time steps of 40 s and 30 s are shown in these figures to make the diagrams clearer. These model predictions were calculated assuming the existence of symmetry and are superimposed with the experimental isochrones.

As can be seen, a good overall adjustment between the model's predictions and the observed fire perimeter was obtained in both scenarios, indicating that the semi-empirical model of fireline rotation and extension provides an adequate prediction of the evolution of the point ignition fire from its initially circular shape to a sort of ellipse with more straight linear shape flanks, as observed in the laboratory experiments and many full-scale fires.

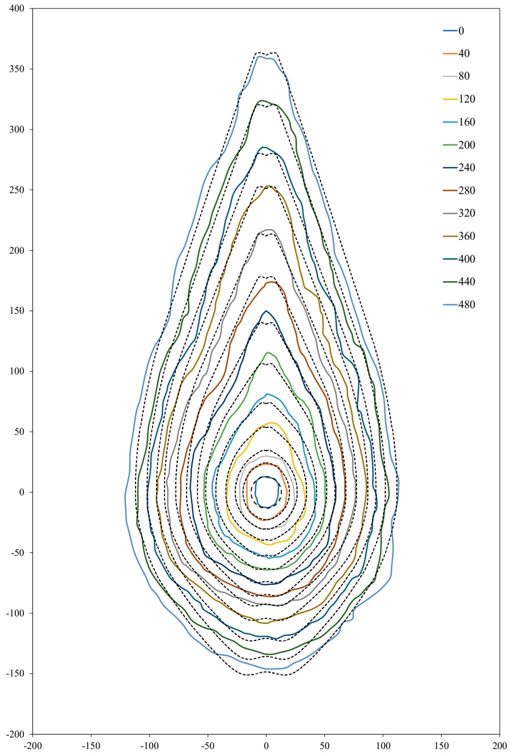

Figure 13. Comparison between fireline contours at 40 s interval obtained from experimental test (continuous line) and with present simulation model (dotted line), for a slope angle of 30°. Dimensions indicated are in cm. Time of each isochrone is specified in legend.

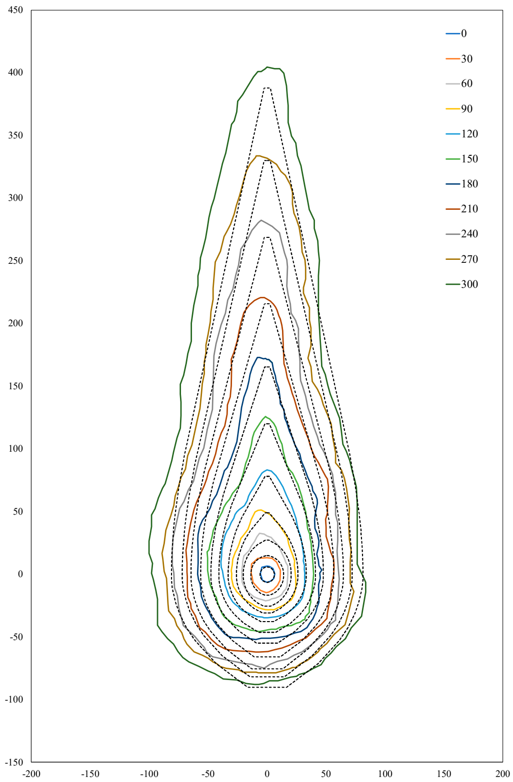

Figure 14. Comparison between fireline contours at 30 s intervals obtained from the experimental test (continuous line) and with present simulation model (dotted line), for a slope angle of 40°. Time of each isochrone is specified in legend.

5. Discussion

The use of the experimental instantaneous values of the reference ROS R_1, R_2, and R_3 is justified by the objective of the present model, which aims to predict the evolution of the overall shape of the fireline using the proposed concepts of rotation and extension, rather than to solely predict their respective ROS values. The experiments conducted reveal that the values of R_i vary over time in a manner that is not accounted for by current models. For example, [13] predicts a constant value for the ROS in this scenario. Even a monotonic variation of R with time would not provide an accurate estimation of the model parameters in the prediction of the two studied cases.

In this study, only a visual adjustment of the fireline sections was conducted to achieve a continuous and closed fireline. This was achieved by modifying the values of A_w and k_e over two or three adjustment steps. It was observed that the model exhibits low sensitivity to changes in the value of m_1, so this parameter was not modified in most cases. The adjustment was performed only to ensure closure of the fireline without regard to its actual shape and conformity with experimental results or the instantaneous values of the relevant ROS.

The necessity for a more refined adjustment process of the parameters is arguable, considering that the shape of the firelines are never regular lines, and perfectly symmetrical firelines are only found in mathematical models. The images shown in Figures 8 and 9, derived from tests conducted under highly controlled laboratory conditions with regular and uniform fuel beds, show that the contour of the burned area is not a regular line but rather a zigzag shape, as advocated in [30]. This irregularity arises from local small-scale convective processes that are not accounted for in the present model.

Using physical considerations, it may be possible to derive relationships among the various parameters for each case. For example, it can be expected that both A_w and k_E must depend on the relevant ROS value or its variation (increase or decrease). To assess this hypothesis, the temporal evolution of each pair of parameters A_w-R and k_E-R for both configurations was analysed in the following figures, separately for the head fire and backfire sections. In the case of the head fire section, the value of R_1 serves as the prevailing or reference ROS value for that section, while for the backfire, R_2 is used.

As shown in Figure 15a,c for the head fire section, the value of A_w closely follows the variations of R_2 at the beginning, but after some time, it decreases to very low values. This result indicates that after a certain threshold, the crossflow velocity u_y decreases at the fireline elements, leading to very low values of A_w.

For the backward section of the fire, Figure 15b,d show that the variations of A_w closely follow those of R in both cases. This result confirms the indication that for low values of R, there is possibly a linear relationship between A_w and R. As can be seen in Figure 15, the values of A_w that were used in the simulation of the two cases are in the range of those measured independently for these experimental conditions.

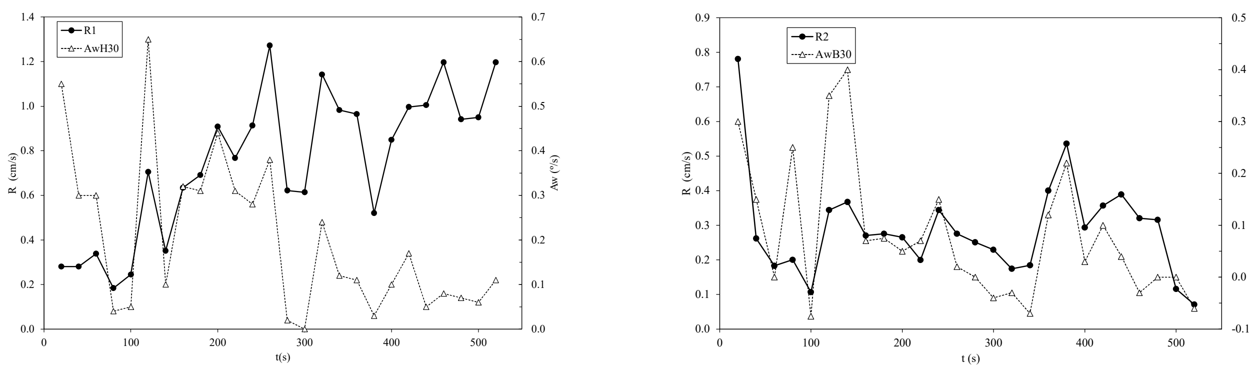

(**a**) (**b**)

Figure 15. *Cont.*

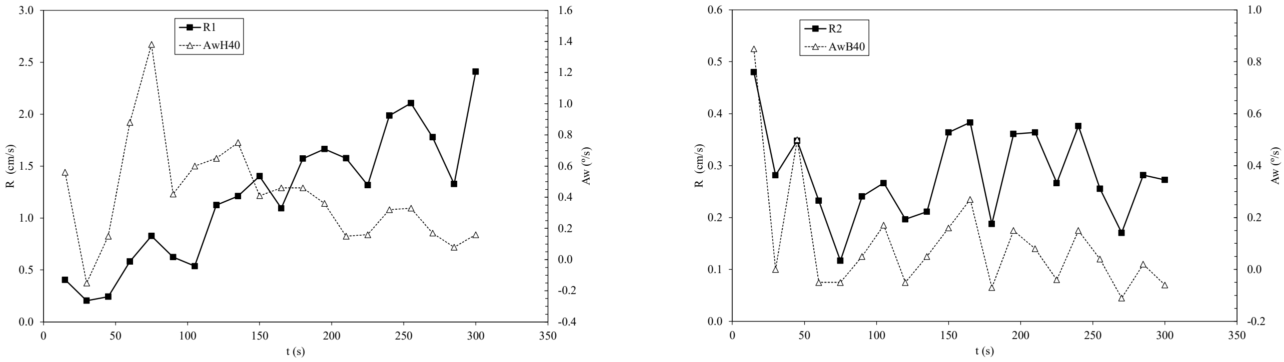

(**c**) (**d**)

Figure 15. Temporal evolution of relevant ROS and of A_w parameter: (**a**) α = 30° Section 1; (**b**) α = 30° Section 2; (**c**) α = 40° Section 1; and (**d**) α = 40° Section 2.

In Figure 16, the temporal variation of the correction coefficient k_E is shown for the four cases, along with the relevant ROS as shown in Figure 15. Its value is always in the same order of magnitude, ranging between 0.2 and 2.4. In the case of the head fire section (Figure 16a,c), the value of k_E appears to increase with R_1 for the two slope angles. Conversely, for the backward section of the fire (Figure 16b,d), there is not a clear tendency of variation of k_E with R_2.

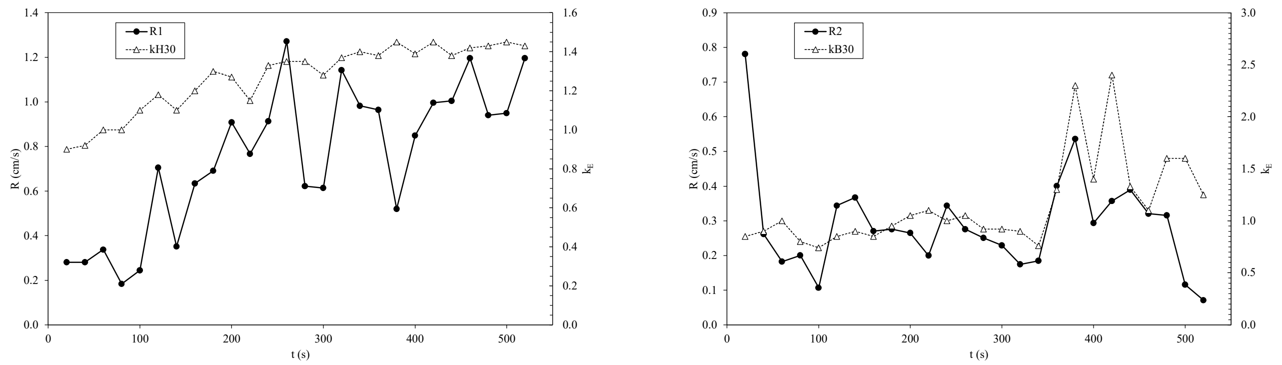

(**a**) (**b**)

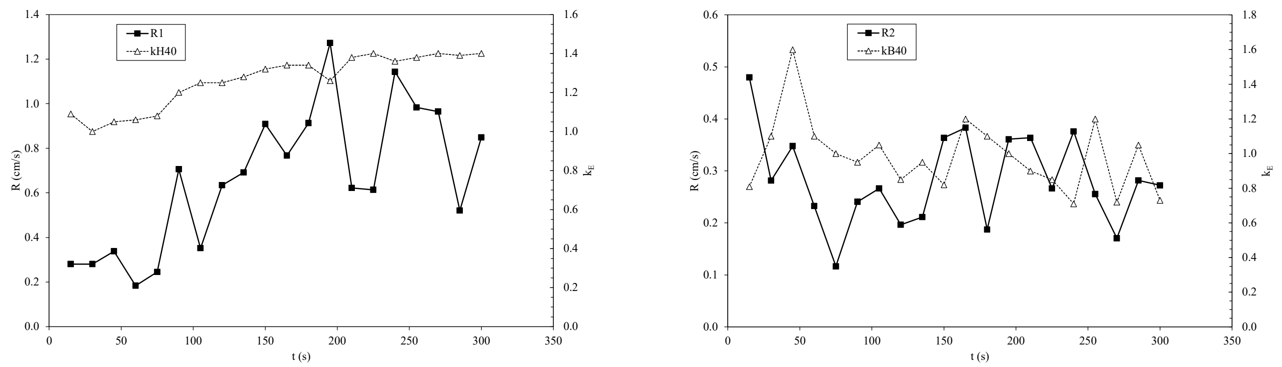

(**c**) (**d**)

Figure 16. Temporal evolution of relevant ROS and of k_E parameter: (**a**) α = 30° Section 1; (**b**) α = 30° Section 2; (**c**) α = 40° Section 1; and (**d**) α = 40° Section 2.

Figures 17 and 18 show the relationship between the four parameters considered with their respective ROS values: A_{wH} and k_{EH} with R_1, and A_{wB} and k_{EB} with R_2. Within the range of the present experiments, it becomes apparent that there is not a monotonous growth of either parameter with R.

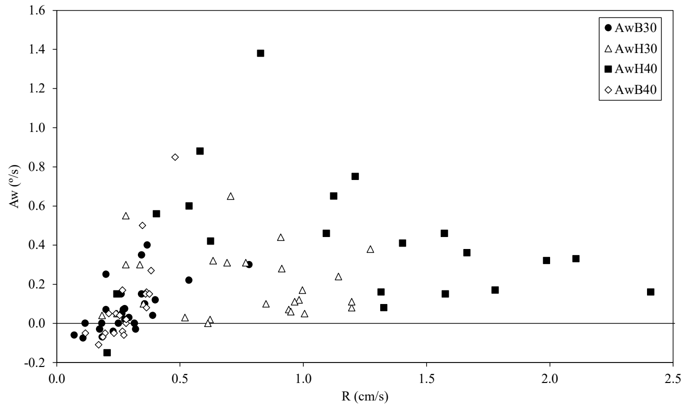

Figure 17. Relationship between A_w and dominant ROS.

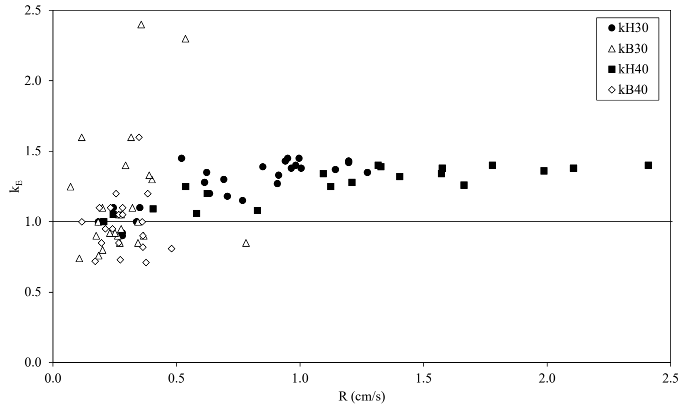

Figure 18. Relationship between k_E and dominant ROS.

For lower values of R, A_w increases to a value close to 1 °/s when the ROS value is close to 1 cm/s for these fuel bed and test conditions. Subsequently, the value of A_w decreases continuously. The scatter of the data prevents the proposal of a mathematical model for this parameter. The corrective coefficient k_E has a similar behaviour, increasing for values of $0 < R < 1$ cm/s. However, for larger values of R, it remains close to 1.4 without decreasing.

By applying an optimization algorithm to a large number of cases, it would become possible to derive more precise dependence laws among these parameters and potentially support the model's generalization to other scenarios.

6. Conclusions

In this study, we present a mathematical model designed to predict the evolution of the fire perimeter using the concepts of fireline rotation and extension. We validate this model using data from two experimental fires involving point ignition on a slope with uniform properties. Our approach employs a semi-empirical model to estimate the rotational velocity of FLEs, which is based on the physical process of convective heat transfer along the fire front. Additionally, we propose a semi-empirical formulation of the fireline extension along the fire perimeter using a simple one parameter power law. The model parameters can be obtained from experimental data. Despite the small database explored, we observed that the model effectively predicts the evolution of the fire perimeter in the studied cases.

The current results were obtained using a relatively straightforward numerical algorithm, where model parameters were automatically adjusted. A Python program is currently being developed to better calculate the rotation and extension of the fireline elements. This program aims to systematically adjust the four model parameters and employ quantitative and objective criteria to evaluate the fitness of the model.

The program is intended to calculate the evolution of various fires, aiming to better understand and describe the range of variation of the model parameters across a range of conditions. Initially, experimental laboratory or field scale fires will be analysed, and will subsequently be used on real scale fires to establish a library of boundary conditions and corresponding model parameters. This will enable us to predict the evolution of fires under general conditions.

In future work, the extension of the model to other situations, namely to field and real scale fires, will be pursued. Machine learning methods will be employed to establish relationships between the model parameters and the specific boundary conditions of each fire. Emphasis will be put on analysing the rotation and extension of fireline elements across a wide range of conditions, aiming to generalise the fire prediction model. This will allow an alternative to the current formulation based on elliptical fire growth.

Author Contributions: Conceptualization: D.X.V.; formal analysis: D.X.V., C.R., T.F.B., T.R. and L.M.R.; data curation: C.R., T.F.B., T.R. and L.M.R.; methodology: D.X.V. and C.R.; writing—original draft: D.X.V.; C.R.; writing—review and editing: D.X.V., C.R., T.F.B., T.R. and L.M.R. All authors have read and agreed to the published version of the manuscript.

Funding: This research was funded and carried out within the scope of the following projects: (1) FirEUrisk project—Developing a Holistic, Risk-Wise Strategy for European Wildfire Management, which received funding from the European Union's Horizon 2020 research and innovation program under the grant agreement No. 101003890; (2) Smokestorm project, funded by FCT—Foundation for Science and Technology with reference PCIF/MPG/0147/2019 and DOI: 10.54499/PCIF/MPG/0147/2019). This research was also sponsored by national funds through FCT—Foundation for Science and Technology—under project LA/P/0079/2020, DOI: 10.54499/LA/P/0079/2020 (https://doi.org/10.54499/LA/P/0079/2020, accessed on 28 March 2024).

Institutional Review Board Statement: Not applicable.

Informed Consent Statement: Not applicable.

Data Availability Statement: The data that support this study will be shared upon reasonable request to the corresponding author.

Acknowledgments: The support given by Agenda TransForm, (PRR 02/C05-i01/2022), namely through project "CENTRODEC" (*Centro de Apoio à Decisão com Dados Multisensoriais para a Proteção da Floresta*), with the contract of C.R, is gratefully acknowledged. The support given by Nuno Luís, João Carvalho, and António Cardoso in performing the laboratory experiments is gratefully acknowledged.

Conflicts of Interest: The authors declare no conflicts of interest.

Nomenclature

a_1	Empirical parameter in Equations (28) and (30)
a_3	Empirical parameter in Equations (29) and (30)
A_w	Empirical coefficient
b_1	Exponent in Equations (28) and (30)
b_2	Exponent in Equations (29) and (30)
ds	Fireline element extension during a time step
ds_{1a}	Fireline extension of element E_{1a}
ds_t	Fireline extension due to translation
ds_ω	Fireline extension due to rotation
Ei	Fireline element limited by points $\mathbf{P}_i$ and $\mathbf{P}_{i+1}$
FLE	Fireline element
K	Number of fireline elements
k_E	FLE extension correction coefficient
k_o	Constant associated to extension of element E_{1a}
m_1	Empirical parameter of the model
$\mathbf{P}_1$	Point $\mathbf{P}_1$ in the fireline at time step t

$\mathbf{P}_1{}'$	Point $\mathbf{P}_1$ after displacement (translation and rotation) during time step $t + \Delta t$
$\mathbf{P}_1{}''$	Point $\mathbf{P}_1{}'$ after displacement (translation and rotation) during time step $t + \Delta t$
$\mathbf{P}_2$	Point $\mathbf{P}_2$ in the fireline at time step t
$\mathbf{P}_2{}'$	Point $\mathbf{P}_2$ after displacement (translation and rotation) during time step $t + \Delta t$
$\mathbf{P}_2{}''$	Point $\mathbf{P}_2$ after displacement (translation and rotation) during time step $t + \Delta t$
R	Modulus of the ROS
R_1	Head fire ROS
R_2	Backfire ROS
R_3	Lateral fire ROS
R_o	Initial radius of the fire perimeter
Ro	Basic rate of spread in no slope and no wind conditions
ROS	Rate of spread
s	Extension (length) of a fireline element at time step t
s'	Extension (length) of a fireline element at time step t + Δt
$s_{1a}{}''$	Extension (length) of the fireline element $E1_a$ at time step $t + \Delta t$ after translation
t	Time
u	Local flow velocity parallel to fuel bed
u_x	Local flow velocity component parallel to the fireline element
u_y	Local flow velocity component perpendicular to the fireline element
X	Parameter associated to translation
x_i	Coordinate at y axis
$x_i{}'$	Coordinate at y axis at time step t + Δt
Y	Parameter associated to rotation
y_i	Coordinate at y axis
$y_i{}'$	Coordinate at y axis at time step t + Δt
Greek letters	
β	Angle between the local rate of spread and OY_o axis
Δt	Time variation or time step
θ	Angle from the origin of the cartesian plane
θ_i	Radial coordinate associated to each point
ε_c	Corrected fireline extension coefficient
ε_o	Fireline extension coefficient as function of k_o
ε	Fireline extension coefficient
ω	Rotational velocity
ξ	Angular coordinate

References

1. Pastor, E.; Zárate, L.; Planas, E.; Arnaldos, J. Mathematical models and calculation systems for the study of wildland fire behaviour. *Prog. Energy Combust. Sci.* **2003**, *29*, 139–153. [CrossRef]
2. Arroyo, L.A.; Pascual, C.; Manzanera, J.A.; Manzanera, A.; Arroyo, L.A.; Pascual, C. Fire models and methods to map fuel types: The role of remote sensing. *For. Ecol. Manag.* **2008**, *256*, 1239–1252. [CrossRef]
3. Sullivan, A.L. Wildland surface fire spread modelling, 1990–2007. 1: Physical and quasi-physical models. *Int. J. Wildl. Fire* **2009**, *18*, 349. [CrossRef]
4. Sullivan, A.L. Wildland surface fire spread modelling, 1990–2007. 2: Empirical and quasi-empirical models. *Int. J. Wildl. Fire* **2009**, *18*, 369. [CrossRef]
5. Sullivan, A.L. Wildland surface fire spread modelling, 1990–2007. 3: Simulation and mathematical analogue models. *Int. J. Wildl. Fire* **2009**, *18*, 387. [CrossRef]
6. Finney, M.A. *FARSITE: Fire Area Simulator-Model Development and Evaluation*; Res. Pap. RMRS; Department of Agriculture, Forest Service, Rocky Mountain Research Station: Ogden, UT, USA, 1998; pp. 1–36.
7. Finney, M.A. An Overview of FlamMap Fire Modeling Capabilities. In Proceedings of the Fuels Management—How to Measure Success: Conference Proceedings, Portland, OR, USA, 28–30 March 2006; pp. 213–220.
8. Noonan-Wright, E.K.; Opperman, T.S.; Finney, M.A.; Zimmerman, G.T.; Seli, R.C.; Elenz, L.M.; Calkin, D.E.; Fiedler, J.R. Developing the US Wildland Fire Decision Support System. *J. Combust.* **2011**, *2011*, 168473. [CrossRef]
9. Ramírez, J.; Monedero, S.; Buckley, D. New approaches in fire simulations analysis with Wildfire Analyst. In Proceedings of the 5th International Wildland Fire Conference, Sun City, South Africa, 9–13 May 2011; pp. 9–13.
10. Andrews, P.L. Current status and future needs of the BehavePlus Fire Modeling System. *Int. J. Wildl. Fire* **2014**, *23*, 21. [CrossRef]
11. Lopes, A.M.G.; Cruz, M.G.; Viegas, D.X. FireStation—An integrated software system for the numerical simulation of fire spread on complex topography. *Environ. Model. Softw.* **2002**, *17*, 269–285. [CrossRef]

12. Lopes, A.M.G.; Ribeiro, L.M.; Viegas, D.X.; Raposo, J.R. Simulation of forest fire spread using a two-way coupling algorithm and its application to a real wildfire. *J. Wind Eng. Ind. Aerodyn.* **2019**, *193*, 103967. [CrossRef]
13. Rothermel, R.C. *A Mathematical Model for Predicting Fire Spread in Wildland Fuels*; USDA Forest Service, Research Paper INT-115; Intermountain Forest and Range Experiment Station: Ogden, UT, USA, 1972.
14. Rothermel, R.C. *How to Predict the Spread and Intensity of Forest and Range Fires*; Gen. Tech. Rep. INT-143; U.S. Department of Agriculture, Forest Service, Intermountain Forest and Range Experiment Station: Ogden, UT, USA, 1983; 161p.
15. Andrews, P.L. *BEHAVE: Fire Behavior Prediction and Fuel Modeling System-BURN Subsystem, Part 1*; General Technical Report INT-194; U.S. Department of Agriculture, Forest Service, Intermountain Research Station: Ogden, UT, USA, 1986; 130p.
16. Viegas, D.X.F.C.; Raposo, J.R.N.; Ribeiro, C.F.M.; Reis, L.C.D.; Abouali, A.; Viegas, C.X.P. On the non-monotonic behaviour of fire spread. *Int. J. Wildl. Fire* **2021**, *30*, 702–719. [CrossRef]
17. Xavier Viegas, D. A Mathematical Model For Forest Fires Blowup. *Combust. Sci. Technol.* **2004**, *177*, 27–51. [CrossRef]
18. Viegas, D.X. Parametric study of an eruptive fire behaviour model. *Int. J. Wildl. Fire* **2006**, *15*, 169. [CrossRef]
19. Green, D.G.; Gill, A.M.; Noble, I.R. Fire shapes and the adequacy of fire-spread models. *Ecol. Modell.* **1983**, *20*, 33–45. [CrossRef]
20. Richards, G. A General Mathematical Framework for Modeling Two-Dimensional Wildland Fire Spread. *Int. J. Wildl. Fire* **1995**, *5*, 63. [CrossRef]
21. Anderson, D.H.; Catchpole, E.A.; De Mestre, N.J.; Parkes, T. Modelling the spread of grass fires. *J. Aust. Math. Soc. Ser. B Appl. Math.* **1982**, *23*, 451–466. [CrossRef]
22. Alexander, M.E. Estimating the length-to-breadth ratio of elliptical forest fire patterns. In Proceedings of the Eight Conference on Fire and Forest Meteorology, Detroit, MI, USA, 29 April–2 May 1985; pp. 287–384.
23. Richards, G.D. An elliptical growth model of forest fire fronts and its numerical solution. *Int. J. Numer. Methods Eng.* **1990**, *30*, 1163–1179. [CrossRef]
24. Knight, I.; Coleman, J. A Fire Perimeter Expansion Algorithm-Based on Huygens Wavelet Propagation. *Int. J. Wildl. Fire* **1993**, *3*, 73. [CrossRef]
25. Richards, G.D. The Properties of Elliptical Wildfire Growth for Time Dependent Fuel and Meteorological Conditions. *Combust. Sci. Technol.* **1993**, *95*, 357–383. [CrossRef]
26. Johnston, P.; Kelso, J.; Milne, G.J. Efficient simulation of wildfire spread on an irregular grid. *Int. J. Wildl. Fire* **2008**, *17*, 614. [CrossRef]
27. Tymstra, C.; Bryce, R.W.; Wotton, B.M.; Taylor, S.W.; Armitage, O.B. Development and Structure of Prometheus: The Canadian Wildland Fire Growth Simulation Model. 2010. Available online: https://spyd.com/fgm.ca/Prometheus_Information_Report_NOR-X-417_2010.pdf (accessed on 28 March 2024).
28. Viegas, D.X. Fire line rotation as a mechanism for fire spread on a uniform slope. *Int. J. Wildl. Fire* **2002**, *11*, 11. [CrossRef]
29. Oliveras, I.; Piñol, J.; Viegas, D.X. Generalization of the fire line rotation model to curved fire lines. *Int. J. Wildl. Fire* **2006**, *15*, 447–456. [CrossRef]
30. Viegas, D.X. Zigzag shape of the fire front. *Int. J. Wildl. Fire* **2007**, *16*, 763. [CrossRef]
31. Rossa, C.G.; Viegas, D.X. Propagation of Wind and Slope Backfires, 18th World IMACS/MODSIM Congress. 2009, pp. 13–17. Available online: http://mssanz.org.au/modsim09 (accessed on 1 February 2024).
32. Viegas, D.X.; Rossa, C. Fireline rotation analysis. *Combust. Sci. Technol.* **2009**, *181*, 1495–1525. [CrossRef]
33. Viegas, D.X.F.C.; Raposo, J.R.N.; Ribeiro, C.F.M.; Reis, L.; Abouali, A.; Ribeiro, L.M.; Viegas, C.X.P. On the intermittent nature of forest fire spread—Part 2. *Int. J. Wildl. Fire* **2022**, *31*, 967–981. [CrossRef]
34. André, J.C.S.; Gonçalves, J.C.; Vaz, G.C.; Viegas, D.X. Angular variation of fire rate of spread. *Int. J. Wildl. Fire* **2013**, *22*, 970. [CrossRef]